**Noname manuscript No.**
(will be inserted by the editor)

# Capacity of unreinforced rammed earth walls subject to lateral wind force: elastic analysis vs. ultimate strength analysis

**D. Ciancio · C. Augarde**

Received: date / Accepted: date

**Abstract** Cement-stabilized rammed earth walls are an increasingly common form of construction in certain parts of the world, bringing considerable potential to reduce the carbon footprints of buildings. However, there is relatively little advice to designers wishing to use these construction materials at present, as compared to established materials such as concrete. This paper discusses the use of two proposed analysis procedures to calculate the capacity of unreinforced cement-stabilized rammed earth walls to lateral wind force. The first is an elastic analysis while the second is an ultimate strength analysis where a cracked wall is studied as a rigid-body mechanism. The accuracy of each method is assessed against the results of an experimental programme conducted on different rammed earth walls showing the shortcomings of the ultimate strength analysis. A new method is proposed in which the fracture energy required to open the crack that leads to the failure mechanism is included, leading to much improved predictions. The parameters used in the revised ultimate strength analysis are critically discussed and compared to those found in the concrete and masonry literature.

**Keywords** Rammed earth · weak concrete · wind loading · structural analysis.

D. Ciancio
University of Western Australia, M051, 35 Stirling Highway, 6009 Crawley, WA, Australia
Tel.: +61-8-64883892
Fax: +61-8-64881018
E-mail: daniela.ciancio@uwa.edu.au

C. Augarde
School of Engineering and Computing Sciences, Durham University, Durham DH1 3LE, UK

## 1 Introduction

Due to increasing concerns amidst a degrading environment and the unsustainable use of natural resources, the antique rammed earth technique has gained (or regained) a certain popularity in Australia, France and the southern United States since the early 1970s [1]. This renewed interest is most obvious in Western Australia where, in that same period, rammed earth managed to capture 20% of the new building market in the Margaret River Shire [2]. The revival of rammed earth has triggered research into earthen architecture conservation and construction [3, 4]. However to date, after almost 40 years, there has been limited research conducted into the fundamental properties of rammed earth compared to other building materials such as concrete and steel. It is this lack of understanding of the material and its structural behavior that has prevented progress in the development of national standards in many countries, including Australia.

Currently, three Australian advisory documents exist that give advice and guidance on rammed earth aimed at engineers and builders [5–7] but, although useful in many ways, they do not carry the same weight as a standard and they do not offer proper and exhaustive design recommendations for structural members such as walls and lintels. This lack of a standard has led builders and engineers to rely on 'rules of thumb' to design rammed earth structural members. Although widely accepted and used, these rules may lead to the use of unnecessarily large safety factors and consequently unnecessary increases in construction costs.

The development of a standard for design must rely on proven analysis procedures. The aim of this paper is to compare two design methods: an elastic analysis and an ultimate strength analysis. The particular problem on which they are tested is the lateral loading of a free-standing wall. They are used to predict the maximum wind pressure that can be resisted by an unreinforced cement-stabilized rammed earth wall. The analytical results are validated through an experimental programme.

In the following section, the fundamentals of the two analysis approaches are explained. The details of the experimental programme (including soil characterization, walls' boundary conditions and sample preparation) are then presented in Section 3. The experimental results are discussed and then compared with the analytical data in Section 4, showing that the elastic method can accurately predict the capacity of the wall whereas the ultimate strength analysis as presented in Section 2.2 significantly underestimates the maximum wind load that the wall can resist. In Section 5, the ultimate strength analysis is modified to take into account the contribution of the energy dissipated to open the crack that generates the failing mechanisms, leading to a major improvement in accuracy.

## 2 Method

The following assumptions and limitations apply in the study presented in this paper:

- In Australia the use of lintels in rammed earth structures is not frequent. It is a common practice to extend windows and doors to the full height of the wall. For this reason, the model used here represents a wall without any opening of a certain height $h$, thickness $t$ and length $d$.
- It is assumed that the roof system and/or the edge beam at the top of the wall are stiff enough to be modelled as rigid supports.
- The external loads applied to the wall are the horizontal wind pressure $w_f$, the weight of the roof $P$ and the self weight of the wall $W$. The true wind pressure distribution on a wall is complex [8] and in this paper, the negative pressure inside the building and the uplifting force generated by the wind are not considered. The wind pressure is assumed uniformly distributed along the height of the wall. The force $P$ representing the weight of the roof is assumed not to present any significant eccentricity.

### 2.1 The elastic analysis

The model used for this analysis is presented on the left of Figure 1. At failure it is assumed that the rotation of the bottom face of the wall sets the vertical reaction to be eccentric and applied at the edge of the wall. It is unrealistic to expect that the wall will completely detach from the ground slab. Therefore the deformation assumed (as shown in the centre of Figure 1) represents an extreme but conservative scenario. It also assumed that the horizontal reaction $R_2$ at the base of the wall does not exceed the static frictional force equal to $\mu(W+P)$ where $\mu$ is the coefficient of friction between the wall base and its foundation.

From consideration of the global equilibrium for horizontal and vertical forces and moments, the three reactions as shown in Figure 1 are equal to:

$$R_1 = P + \gamma thd;\ R_2 = w_f d\frac{h}{2} + \frac{Pt}{2h} + \frac{\gamma t^2 d}{2};\ R_3 = w_f d\frac{h}{2} - \frac{Pt}{2h} - \frac{\gamma t^2 d}{2} \quad (1)$$

where $\gamma$ is the unit weight of the material (rammed earth). The tensile stress at any cross section along $y$ on the face of the wall is given by:

$$\begin{aligned} &\sigma_T(y) = \frac{M(y)t}{2I} - \gamma y - \frac{P}{td} \\ &\text{with}\ \ M(y) = \frac{-y(Pt + dh(w_f y + t^2\gamma - hw_f))}{2h}\ \ \text{and}\ \ I = \frac{dt^3}{12} \end{aligned} \quad (2)$$

The steps in the elastic analysis are: 1) finding the location $y'$ where the tensile stress is maximum ($\frac{\partial \sigma_T}{\partial y} = 0 \Rightarrow y'$) and 2) calculating the value of $w_f$,

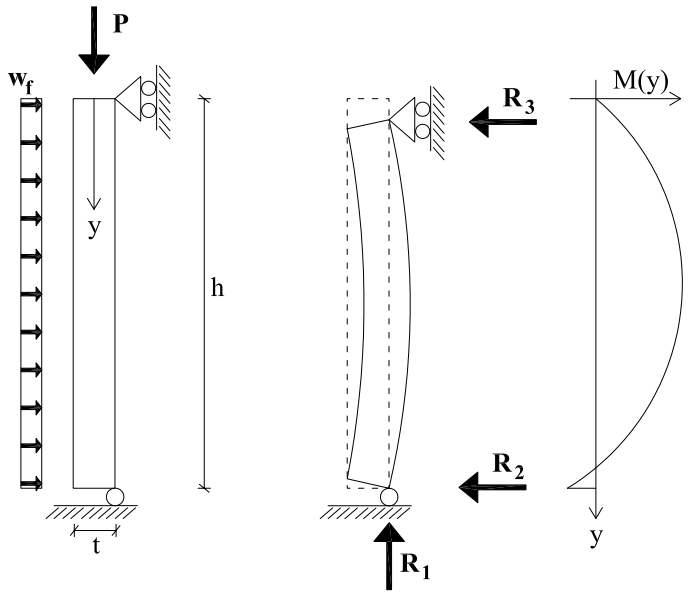


**Fig. 1** Scheme used for the elastic analysis. On the left, boundary conditions; at the centre: possible elastic deformation; on the right: bending moment diagram.

such that the maximum tensile stress equals the tensile strength $f_t$ ($\sigma_t(y = y') = f_t \Rightarrow w'_f$ ). The maximum wind pressure that the wall can resist and the location of the crack at failure are then given by:

$$\begin{aligned} w'_f &= \frac{5Pt + 2dt^2(f_t + 2h\gamma) + 2t\sqrt{(P + dtf_t)(4P + dt(f_t + 4h\gamma))}}{3dh^2} \\ y' &= \frac{hP + dhf_t t + h\sqrt{(P + dtf_t)(4P + dt(f_t + 4h\gamma))}}{5P + 2dt(f_t + 2h\gamma) + 2\sqrt{(P + dtf_t)(4P + dt(f_t + 4h\gamma))}} \end{aligned} \tag{3}$$

## 2.2 The ultimate strength analysis

This method has been used previously for the analysis of masonry walls [9, 10] and rammed earth walls [11]. The onset of a two-rigid-block mechanism, as presented in Figure 2c), is determined by applying the principle of virtual work ($PVW$).

The failure mechanism of the cracked wall can be studied as a structure made of two beams connected by an internal hinge, as shown in Figure 2b). The centres of rotation are $C_1$ and $C_2$ for the upper and lower parts of the wall respectively. The virtual angles of rotation are $\beta$ and $\theta$ with respect to

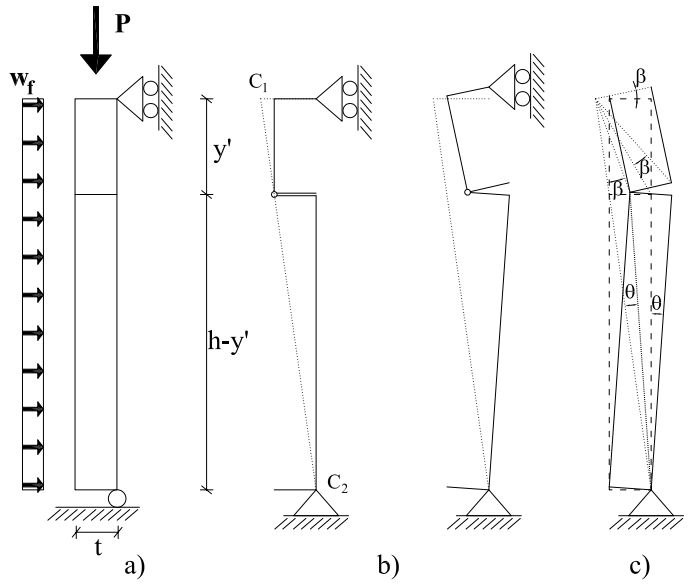


**Fig. 2** Mechanism at failure for a rammed earth wall: a) boundary conditions; b) possible deformed configuration of a wall modeled as made of 2 beams; c) angles of rotation around $C_1$ and $C_2$.

$C_1$ and $C_2$ as shown in Figure 2c). By applying the $PVW$, we obtain:

$$\begin{aligned} &w_f d(h-y')\frac{h-y'}{2}\theta + w_f d\frac{y'^2}{2}\beta - \gamma dt(h-y')\frac{t}{2}\theta + \\ &-\gamma dty'(\frac{t}{2}+\frac{y'}{h-y'}t)\beta - P(\frac{t}{2}+\frac{y'}{h-y'}t)\beta = 0 \quad \forall\ \theta,\beta. \end{aligned} \tag{4}$$

From geometrical considerations $\beta = \frac{h-y'}{y'}\theta$. Therefore, the previous equation is true $\forall\theta$ when:

$$w_f = \frac{t(hP + Py' + 2dhty'\gamma)}{dy'(h^2 - hy')}. \tag{5}$$

The value of $y'$ for which $w_f$ is a minimum indicates the position of the crack at failure. The corresponding value $w'_f$ therefore represents the maximum wind pressure that the wall can resist. From $\frac{\partial w_f}{\partial y'} = 0$, we obtain:

$$\begin{aligned} w'_f &= \frac{t\sqrt{2P(P+dht\gamma)}(P+2dht\gamma)^2}{dh^2(2P+2dht\gamma-\sqrt{2P(P+dht\gamma)})(\sqrt{2P(P+dht\gamma)}-P)} \\ y' &= \frac{h\sqrt{2P(P+dht\gamma)}-hP}{P+2dht\gamma}. \end{aligned} \tag{6}$$

## 3 Experimental programme

### 3.1 Wall testing

To check the accuracy of the methods presented in the previous section, three walls of height $h$ 1200mm, length $d$ 600mm and varying thicknesses $t$ of 50, 100 and 150mm were tested. The testing frame shown in Figure 3a) was a modification of the steel box (Figure 3b)) initially used to ram each wall, in which one side of the formwork was removed. An airbag chamber constructed from plywood was housed at the back of the frame to contain an airbag which simulated the wind force, as shown in Figure 3c). The airbag loading was measured by a pressure transducer. The wall simply stood on the floor in front of the airbag chamber with its top and bottom restrained by 2 rigid bars of the frame, as shown in Figure 3d). These are the only restraints that the wall experienced that are assumed to act as a pin at the bottom and a roller at the top of the wall. It is realistic to think that the friction between the steel bar and the rammed earth wall might restrain the vertical displacements at the top of the wall. In that case, it would have been more appropriate to model the experimental setup using the scheme in Figure 1 with a vertical confining spring at the roller at the top of the wall. However, experimental evidence indicated that the vertical movements of the wall were not constrained. Furthermore, the contact surface between the horizontal steel bar and the rammed earth surface is relatively small. For this reason, any friction effect was neglected.

The steel frame was bolted to the ground. The vertical load $P$ was applied by positioning 2 steel bars at the top of the wall and by clamping them to the rigid frame, as shown at the top of Figure 3e). Between the 2 bars, a load cell was inserted. The clamping was manually operated and stopped when the load cell showed the desired value of $P$ that was then kept constant during the testing. The airbag was then slowly and steadily inflated until the failure of the wall was reached.

### 3.2 Soil mix

The rammed earth mix used is representative of one commonly used by rammed earth contractors in Perth, Western Australia. It consists of 19mm (max. size) crushed limestone (with the particle size distribution shown in Figure 4) 8% of cement by limestone weight and water content of approximately 8.2%. The optimum water content was calculated using the drop test method [5,6], where a ball is made in the palm using a small sample of the mix and is dropped from a height of 1100mm. If the ball shatters into many small fragments, water content is adequate to achieve max compaction and if it shatters into a few large pieces, it is too wet. When the soil is too dry, the soil cannot be pressed into a ball. Water was added depending on the results of the drop test and the mixer allowed to rotate for another minute before a second drop test was conducted.


**Fig. 3** Experimental setup. a): steel frame constraining the rammed earth wall; b): ramming formwork; c): top view of the not fully inflated airbag; d): complete experimental scheme; top of e): clamped steel bars generating the pre-load $P$.

Even though the designed material mix was the same for the three walls, there are likely to be minor variations between the batches. For this reason, from here the three mixes used for wall 1 (50mm thickness), wall 2 (100mm thickness) and wall 3 (150mm thickness) will be indicated as batches 1, 2 and 3 respectively. Small samples were taken from each batch and weighed before and after drying in an oven to calculate the water content in the mix. The water content of batch 1 was 7.6%, batch 2 8% and batch 3 8.4%. However, the weight loss in the oven does not take into account the non-evaporable water consumed in the hydration process of the cement, triggered by the high temperature ($100^o$) of the oven. For 8% cement content, this non-evaporable water was calculated as 2% of the 'fictitious' water contents. The real water content of the rammed earth batches is then equal to 7.8% for batch 1, 8.2% for batch 2 and 8.5% for batch 3.

The material was placed in the formwork in amounts that would achieve compacted layers of 100mm height. A 'Bosch GSH 11 E Professional' jackhammer was used with a square hammer plate of 50, 100 and 150mm respectively

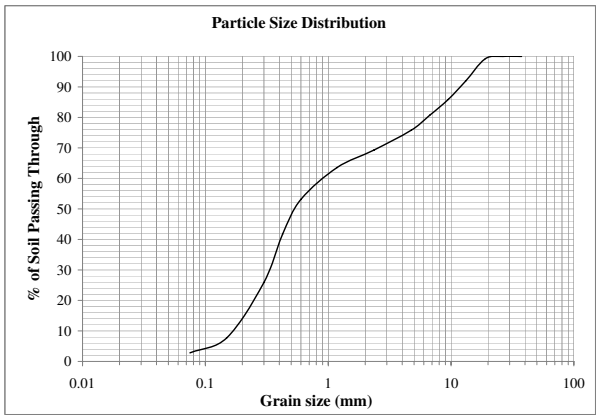


**Fig. 4** Particle size distribution of the 19mm (max size) crushed limestone used for the rammed earth mix.

for each wall. After each layer was compacted, the surface was roughened to ensure a good bond with the next layer.

### 3.3 Mechanical material parameters

The experimental programme also included the calculation of some mechanical properties of the material mix. Table 1 shows the tests performed on moulded and cored samples. Using similarities between concrete and cement-stabilized rammed earth [12], the indirect tensile strength (ITS) and the flexural tensile strength (FTS) were calculated following the recommendations in concrete standards [13–15].

- To calculate the unconfined compressive strength (UCS), cylindrical rather than prismatic samples were used [5] of diameter 100mm and height 200mm. The dimensions of the samples cored from the intact parts of the wall change according to the thickness of the walls, as shown in Table 1.
- The indirect tensile strength was obtained from moulded cylindrical samples of 150mm diameter and 300mm height. The test was carried out according to AS 1012.10 [14]. The details of this experimental test are not discussed in this paper, since they are well-known and understood procedures commonly used for concrete. It is important to underline, however, the position of the ramming lines in the sample with respect to the direction of the vertical tensile crack, as shown in Figure 5.
- The flexural tensile strength was obtained through the third-point loading method [15]. For this purpose, some beamlets were cored from the intact parts of the walls, and tested according to the scheme presented in Figure

| | moulded samples | | | | cored samples | | | |
|---|---|---|---|---|---|---|---|---|
| | unconfined compressive strength UCS | | indirect tensile strength (ITS) | | unconfined compressive strength UCS | | flexural tensile strength (FTS) | |
| batch | # samples | dimension samples [mm] | # samples | dimension samples [mm] | # samples | dimension samples [mm] | # samples | dimension samples [mm] |
| 1 | 1* | $\Phi 100 \times 200$ | 1* | $\Phi 150 \times 300$ | 6 | $\Phi 30 \times 60$ | 4 | $50 \times 50 \times 200$ |
| 2 | 3 | $\Phi 100 \times 200$ | 3 | $\Phi 150 \times 300$ | 6 | $\Phi 40 \times 80$ | 4 | $100 \times 100 \times 400$ |
| 3 | 3 | $\Phi 100 \times 200$ | 3 | $\Phi 150 \times 300$ | 5 | $\Phi 80 \times 160$ | 3 | $150 \times 150 \times 400$ |

**Table 1** Experimental programme to calculate rammed earth mechanical parameters (*A minimum of three cylinders per batch is recommended in order to obtain reliable test results for the UCS and ITS test. This was not possible for wall 1 due to a mistake during the batching process.

**Fig. 5** Experimental setup for the indirect tensile strength test.

6a). This test aimed to determine the tensile strength at the interface of the rammed layers. Due to some geometry-constraints of wall 1 after failure, the beamlets cut there were only 200mm long and contained only one ramming line. For these beams, the three-point bending test was used, as shown in Figure 6b). A minimum of three cylinders per batch is recommended in order to obtain reliable test results for the *UCS* and *ITS* test. This was not possible for wall 1 due to a mistake during the batching process.

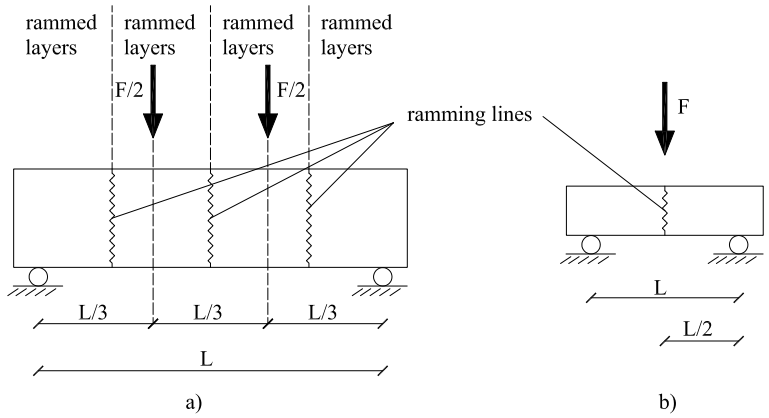


**Fig. 6** Experiment to calculate the flexural tensile strength: a) third-point loading bending test; b) three point bending test.

## 4 Experimental results

After being rammed, the 3 walls were left to dry in the formwork for two days. Once de-moulded, they were wrapped in plastic bags for 7 days and then cured in ambient conditions. The walls were tested after 28 days. The unit weight $\gamma$ of the walls at 28 days was calculated as 18.64 $kN/m^3$. This value was used in Equations 3 and 6.

### 4.1 Unconfined compressive strength

The results of the unconfined compressive strength tests are presented in Figure 7. A size effect similar to the one shown by concrete samples [16] might explain the difference in strength amongst the cored samples, i.e. the bigger the sample, the lower the strength. There are not enough results of moulded specimens of batch 1 to comment. The variation in strength between the moulded samples of batch 2 and 3, and the cored samples of batch 1, 2 and 3 might be due to the different water contents (wc) in each batch (indicated in the graph). Soil samples compacted at or below their Optimum Water Content tend to perform better than samples compacted at higher water content.

### 4.2 Indirect tensile strength

The results of the indirect tensile strength tests are presented in Figure 8. There seems to be an agreement between the three batches in terms of average indirect tensile strength. In these tests it is important to note that the tensile

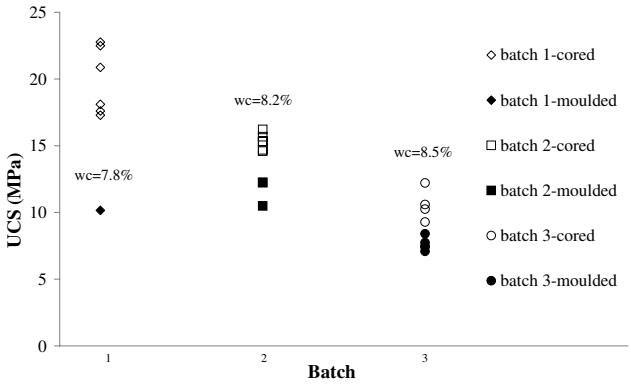


**Fig. 7** Unconfined compressive strength of cored and moulded samples from batch 1, 2 and 3.

strength measure is that of material within the rammed layers and not the strength of the interface between layers.

### 4.3 Flexural tensile strength

The flexural tensile strength test was designed to measure the tensile strength at the interface between rammed layers, i.e. the so-called ramming line. The results (plotted in Figure 9) show that, as expected, the tensile strength at these lines is smaller than the indirect tensile strength presented in Figure 8. The high variability of results between the 3 batches and within the samples of batch 2 might be due to the fact that the specimens for this test were cored from the walls. The coring process might have damaged or altered the structure of the samples. Similar variability was found in other studies on cored samples [17].

### 4.4 Maximum horizontal pressure on wall

The vertical force $P$ applied at the top of the wall corresponds to the weight of a terracotta tiled roof. For the 1:2 scaled walls used in this experimental programme, the value of $P$ was calculated to be 1.48 kN. Since this pre-load was manually applied (as explained in Section 3.1), small differences in $P$ were unavoidable between the 3 walls, as presented in Table 2. The airbag pressure was slowly increased until failure, as shown in Figure 10. Table 2 presents

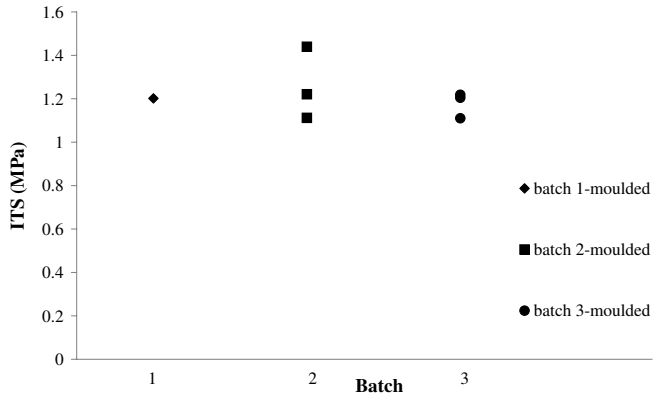


**Fig. 8** Indirect tensile strength of moulded samples from batch 1, 2 and 3.

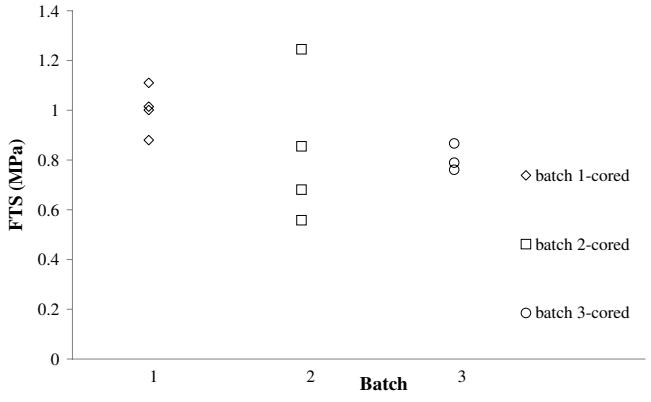


**Fig. 9** Flexural tensile strength for cored samples of batch 1, 2 and 3.

the experimental values of the airbag pressure at failure (column 4), together with the analytical values of the maximum wind pressures $w'_f$ obtained by the elastic analysis (Equations 3) in column 6 and the ultimate strength analysis (Equations 6) in column 8. For the elastic analysis, the tensile strength $f_t$ is equal to the mean value for each batch of the data presented in Figure 9.

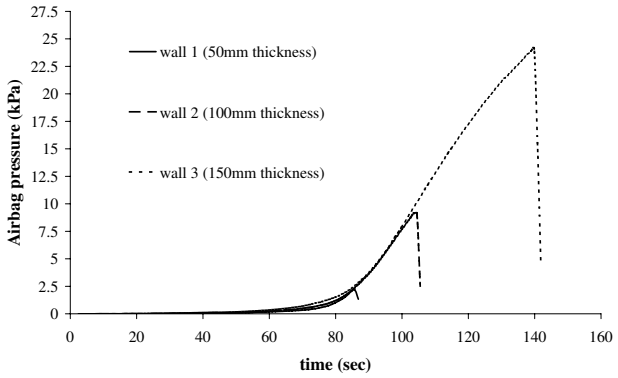


**Fig. 10** On the left: Airbag pressure vs. time curves for wall 1, 2 and 3. On the right: failure mode of wall 3.

| | experimental values | | | | Elastic analysis Eqs. 3 | | Ultimate strength analysis Eqs. 6 | |
|---|---|---|---|---|---|---|---|---|
| | P [kN] | $f_t$=average FTS [MPa] | airbag pressure at failure [MPa] | distance of crack from top [m] | $w'_f$ [kPa] | y' [m] | $w'_f$ [kPa] | y' [m] |
| wall 1 | 1.46 | 1.001 | **2.14** | 0.61 | **2.69** | 0.569 | **0.62** | 0.439 |
| wall 2 | 1.48 | 0.834 | **9.41** | 0.58 | **8.69** | 0.573 | **1.52** | 0.401 |
| wall 3 | 1.55 | 0.806 | **24.16** | 0.43 | **18.60** | 0.576 | **2.73** | 0.376 |

**Table 2** Maximum wind pressure and crack location: experimental vs. analytical results

### 4.5 Discussion on elastic analysis vs. ultimate strength analysis

It is evident from Table 2 that the ultimate strength analysis fails dramatically to predict the capacity of the wall to resist the horizontal wind pressure, significantly underestimating the ultimate wind force. This might be due to the fact that the work balance in Equation 4 does not take into account the energy necessary to create a crack along the wall, required for the conversion of the wall into a mechanism. The ultimate strength method is clearly more suitable for the analysis of gravity walls, in which no energy is required to open the interface between two blocks, or for masonry walls in which the mortar layers are far weaker than the bricks. Despite this, it is interesting to note that when $P = 0$, the value of $w_f$ for which Equation 4 is equal to zero is $2t^2\gamma/(h - y')$. This is an increasing function of $y'$ whose minimum value is $w'_f = 2t^2\gamma/h$ for

$y' = 0$. This leads to the result that for $P = 0$, the crack should appear at the top of the wall ($y' = 0$) when using the ultimate strength analysis as presented in Equation 6. This is however reasonable if one considers that if $P = 0$ the wall is then subject to prestress only from self-weight, which will therefore be a maximum at the base and zero at the top.

The elastic analysis, in contrast, produces a realistic simulation of the ultimate airbag pressure on the walls. It is reasonable to state that if the tensile strength at the ramming lines is accurately calculated, this analysis is able to correctly predict the capacity of the wall. Nevertheless, the result obtained makes it appear that if the tensile strength is not properly estimated the method is error-prone. This is definitely the case for the largest wall (3): a local high strength (greater than measured in the samples) due to the inhomogeneity of the material could have caused the wall to fail away from the centre. However other factors might have influenced this result, one of which could be the aspect ratio of the panel. The elastic analysis is based on Equation 2 and while the aspect ratio for wall 3 lies just outside the requirement of Euler-Bernoulli beam theory (i.e. $t < h/10$) this is not thought to be significant here. Another possibility is potential for the boundary conditions to vary slightly between tests, perhaps due to different loadings leading to changes in friction between the base of the wall and the support, although these would be very difficult to assess in practice.

Figure 11 shows an inverse analysis of the results for wall 3. For the sake of this explanation, some arbitrary values of tensile strength with the same order of magnitude of the experimental results in Figure 8 and 9 have been adopted: at the central third the tensile strength has been assumed to be equal to 1.2MPa and in the lateral thirds equal to 0.96 MPa. Each curve plotted shows the variation of the maximum tensile stress along the wall for increasing values of $w_f$ (Equation 2). For $w_f = 18.60$ kPa, the maximum tensile stress is equal to 0.806 MPa and is attained at point A, where the strength is much higher. No failure is registered at this stage. For $w_f = 21.92$ kPa, the maximum tensile stress is equal to 0.96 MPa at a central location (point B) of the wall where the tensile strength is assumed to be 1.2 MPa. The crack will not open there. Finally, for a wind pressure equal to 24.16 kPa the tensile stress at point C is equal to the tensile strength of 0.96 MPa and the crack opens there. The crack does not open where the tensile stress is maximum, i.e. at point D where $\sigma_T = 1.07MPa$, because the stress at that section is still less than the material strength. The crack will open instead at the weakest tensile strength location. Therefore, if it is assumed that along the lateral ramming lines the tensile strength is lower than the strength at the central part of the wall, the mechanism experimentally observed for wall 3 might be explained. In conclusion, it seems that the evaluation of the tensile strength of wall 3 might not have been accurate and this leads to underestimations in the predictions. It is also worth noting that the beams used in the FTS test were cut *after* the failure of the wall. Consequently they might have been damaged and therefore show a reduced tensile strength.

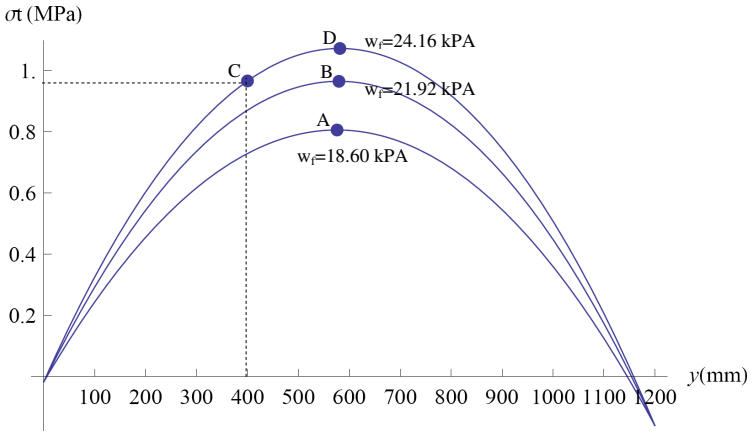


**Fig. 11** Tensile stresses along the extreme fibres of wall 3 vs distance from top of the wall for different values of wind pressure wf. Point A, B and D are maximum values, but the crack forms at point C, probably representing a weak point for wall 3.

Even though maximum attention was expended to guarantee a uniform ramming procedure and consistent conditions at each ramming line, the inverse analysis previously presented demonstrates that there might be some variation of the mechanical properties of the material along the height of the wall. This might compromise the accuracy of the elastic analysis. However, despite this it is clear that the ultimate strength method used previously to predict failure of this nature is even worse and could not to be relied upon.

## 5 Ultimate strength analysis including Mode I fracture energy

In the above we have seen that an elastic analysis provides a better prediction of the experimental results than the ultimate strength analysis, the latter being usually regarded as more sophisticated. Here we examine the effect of considering in addition the work required to open a full-depth crack in the wall, to convert an uncracked wall into the required mechanism. This has been ignored in previous uses of the ultimate strength method.

The cement-stabilized limestone used in these experiments can be reasonably compared to a weak concrete. A good approximation of the stress ($\sigma$)-crack opening displacement ($\delta$) curve along a Mode I cohesive crack in this type of material can be any of the curves shown in Figure 12 [18–20]. The area

under the $\sigma - \delta$ curve represents the fracture energy $g_f$:

$$g_f = \int_0^{\delta_{max}} \sigma d\delta. \tag{7}$$

In this study, it is assumed that at failure the crack opening along the extreme fibres of the wall is equal to $\delta_{max}$ and that the stress distribution along the crack is given by the model in Figure 12c). In other words, it is assumed that, independently from the geometry of the 3 walls, the configuration at failure is the same; that is the wall fails when the maximum crack opening displacement at the extreme fibres is equal to $\delta_{max}$. This situation is reported in detail in Figures 13a) and b). It should be noted that $\delta_{max}$ is a material parameter, equivalent to $w_1$ in Hillerborg *et al.*'s work [20]. The scheme in Figure 13a)

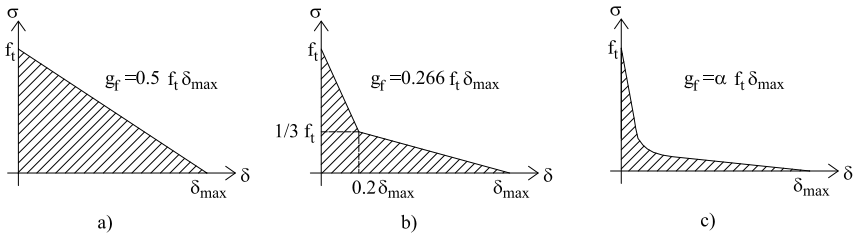


**Fig. 12** Cohesive Mode I crack models: a) and b) proposed by Hillerborg [18] for concrete; c) generic post-crack softening behaviour [18] used in this study for cement stabilized rammed earth.

assumes that the length of the crack is equal to the thickness $t$ of the wall. In reality, the actual length of the crack is less than $t$, as shown in the scheme in Figure 13c), in which part of the wall cross section is under compression and the remaining part is under tension. It is assumed here that at failure the length $z$ (the intact part of the cross section) is negligible with respect to $t - z$ (the cohesive crack length).

Under these new assumptions, Equation 4 (the Principle of Virtual Work) can be re-written adding the contribution of the total virtual fracture energy

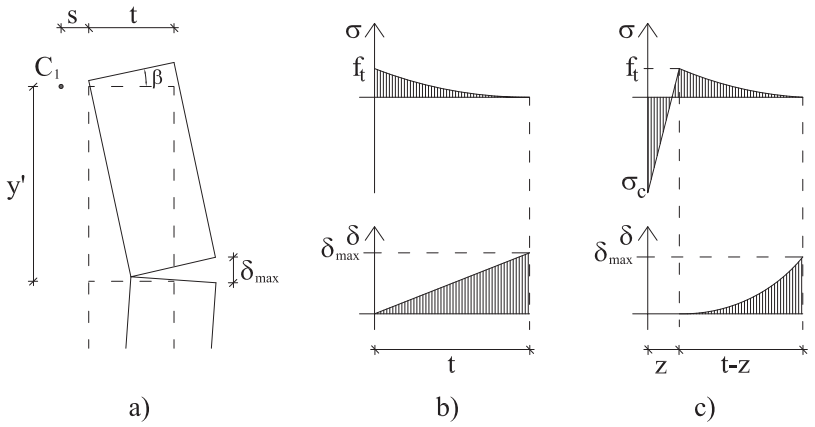


**Fig. 13** a) crack opening at failure; b) assumptions of the stress distribution and crack opening displacement along the thickness of the wall; c) more realistic scheme in which the crack does not entirely propagate through the thickness of the wall.

along the crack which is:

$$\begin{aligned} &w_f d(h-y')\frac{h-y'}{2}\theta + w_f d\frac{y'^2}{2}\beta - \gamma dt(h-y')\frac{t}{2}\theta + \\ &-\gamma dty'(\frac{t}{2}+\frac{y'}{h-y'}t)\beta - P(\frac{t}{2}+\frac{y'}{h-y'}t)\beta - g_f td = 0 \quad \forall\ \theta,\beta \end{aligned} \tag{8}$$

where according to Figure 12c):

$$g_f = \alpha f_t \delta_{max} = \alpha f_t(s+t)\beta = \alpha f_t(\frac{y't}{h-y'}+t)\frac{h-y'}{y'}\theta. \tag{9}$$

being $s$ the distance between the centre of rotation C1 and the edge of the wall (as shown in Figure 13a). Following the same procedure as presented in Section 2.2, the value of the wind pressure that causes the failure of the wall and the position of the crack along the wall are given by:

$$\begin{aligned} w'_f &= \frac{-t(P+2dht\gamma)^2)m}{dh^2((P+2df_t t\alpha)-m)(2(P+df_t t\alpha)+2dht\gamma-m)} \\ y' &= \frac{-h(P+2df_t t\alpha)+hm}{P+2dht\gamma} \end{aligned} \tag{10}$$

where

$$m = \sqrt{2(P+2dtf_t t\alpha)(P+dt(f_t\alpha+h\gamma))} \tag{11}$$

5.1 Results and comparison with the experimental data

The values of $w'_f$ and $y'$ using Equation 10 are plotted against $\alpha$ in Figure 14 for walls 1 to 3. Increasing values of $\alpha$ mean higher material fracture energy, i.e. a higher capacity for the wall to dissipate energy before the complete opening of the crack. The graph on the left of Figure 14 shows that if the material is the same for the three walls, i.e. $\alpha$ is the same, the maximum wind pressure $w'_f$ increases with increasing thickness of the wall. The position of the crack at failure, $y'$, seems not to be significantly affected by the value of $\alpha$ or the thickness of the wall, as the graph on the right of Figure14 indicates. The limit of $y'$ for $\alpha$ tending to infinity is $h/2$.

Further analysis of Equation 10 indicates that when $P = 0$ $w'_f$ is lower than the case for $P > 0$. This result confirms the stabilizing effect of the force $P$ on the capacity of the wall. It is also important to note that when $P = 0$ and $\gamma = 0$ (that is zero compression along the height of the wall), the crack at failure forms at $y' = h/2$ (i.e. the symmetric case for a simply supported beam).

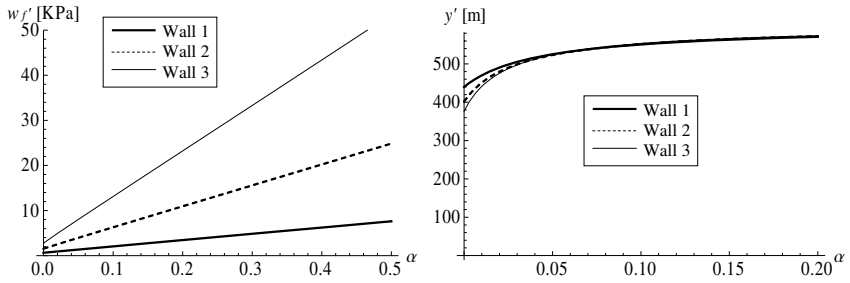


**Fig. 14** Curves representing Eqs. 10 (i.e. $w'_f$ and $y'$ vs $\alpha$).

Table 3 compares the experimental, elastic analysis and revised ultimate strength analysis results for the walls. The results in the last 2 columns were obtained by assigning to $\alpha$ an *ad-hoc* value of 0.15 so that the results obtained with the new formulation of the ultimate strength analysis are in better agreement with the experimental results and also with the analytical results obtained with the elastic analysis. The value of $\alpha$ was arbitrarily chosen because

| | experimental values | | | | Elastic analysis Eqs. 3 | | ultimate strength analysis Eqs. 10 | |
|---|---|---|---|---|---|---|---|---|
| | P [kN] | $f_t$=average FTS [MPa] | airbag pressure at failure [MPa] | distance of crack from top [m] | $w'_f$ [kPa] | y' [m] | $w'_f$ [kPa] | y' [m] |
| wall 1 | 1.46 | 1.001 | **2.14** | 0.61 | **2.69** | 0.569 | **2.74** | 0.563 |
| wall 2 | 1.48 | 0.834 | **9.41** | 0.58 | **8.69** | 0.573 | **8.61** | 0.564 |
| wall 3 | 1.55 | 0.806 | **24.16** | 0.43 | **18.60** | 0.576 | **18.17** | 0.556 |

**Table 3** Maximum wind pressure and crack location: experimental vs. analytical results

it was not possible to obtain an experimental value in this study. However, by taking into account that $\alpha = 0.15$ is a value which is within the range of the material properties for concrete ($\alpha$ can be post-processed from the concrete experimental results from [19,21,22]), and considering the similarities between concrete and cement-stabilised rammed earth, this choice is reasonable. The results in Table 3 show that it is possible that ignoring the fracture energy of the material could be the reason for the poor results obtained with Eq. 6 and shown in Table 2. Further discussion on this matter is presented in the following Section.

### 5.2 Discussion on validity of fracture energy in ultimate strength analysis

The assumptions of the Mode I crack model used for cement-stabilized rammed earth (behavior shown in Figure12c) are discussed here. By exploiting some similarities between cement-stabilized rammed earth and concrete, we aim to validate the proposed method by showing that reasonable figures for $\alpha$ and $\delta_{max}$ exist. As reported in Equation 9, the specific fracture energy $g_f$ is a function of $f_t$ (experimentally calculated in this work), $\alpha$ (arbitrarily taken equal to 0.15) and $\delta_{max}$. At failure $\delta_{max} = (\frac{y't}{h-y'} + t)\frac{h-y'}{y'}\theta$ (as calculated from Figure 13a). Since $\delta_{max}$ is a material parameter, it must be reasonably similar for the three walls, as shown on the left of Figure 15. Using Equation 10 for $y'$, the function $\delta_{max} = \delta_{max}(\theta)$ is plotted on the right of Figure 15 for each wall showing that for a fixed value of $\delta_{max}$ the corresponding $\theta$ changes from wall to wall, with $\theta_1 > \theta_2 > \theta_3$. Following some experimental results obtained for concrete, in this study $\delta_{max}$ is taken equal to $0.15mm$ [21]. For $\delta_{max} = 0.15mm$ and $\alpha = 0.15$, the specific fracture energy $g_f = \alpha f_t \delta_{max}$ turns out to be equal to: 22.50N/m for wall 1; 18.76N/m for wall 2 and 18.13N/m for wall 3. These numbers are in good agreement with experimental data obtained for concrete with similar $UCS$ and $FTS$ [22,23].

The previous analysis is not meant to assign a value to the material properties of cement stabilized rammed earth by an inverse analysis alone. It is obvious that the material parameters $\alpha$ and $\delta_{max}$ need to be validated. This area of investigation requires further experimental research and analysis.

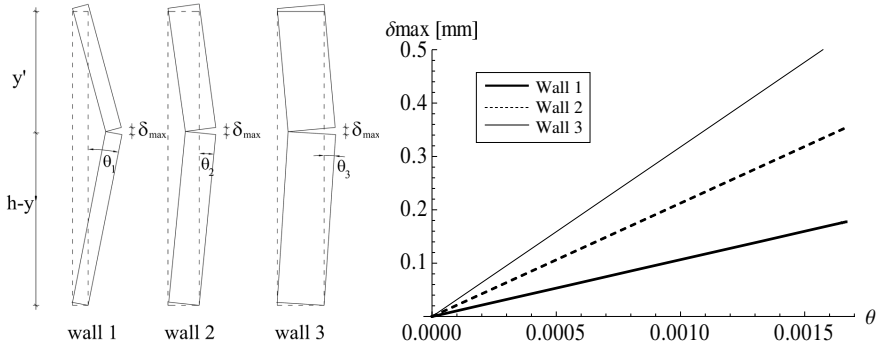


**Fig. 15** On the left, configurations at failure for the three walls. On the right, $\delta_{max}$ vs $\theta$ for the three walls.

Another interesting application of the revised ultimate strength method proposed here regards the analysis of masonry walls. As mentioned in Section 4.5, Equation 6 is more suitable for walls in which there is a layer significantly weak in tension, as are the mortar layers in masonry walls, and Equation 10 is more applicable to cases in which there is a significant energy required to form the crack that leads to the failure mechanism. In Hamoush et al. [24], two concrete masonry walls of dimensions 1200 ($d$) x 1800 ($h$) x 200 ($t$) mm were tested for out-of-plane bending using an experimental rig similar to the one used in this study. The maximum wind pressure at failure was 0.68 kPa for one wall and 1.43 kPa for the other. Here the ultimate strength analysis (with and without the fracture energy contribution) is used to reproduce Hamoush et al.'s experimental findings. The unit weight of the walls is not given, but it is reasonable to assume that it should be in the range between 10 and 24 $kN/m^3$. The graph at the top left of Figure 16 shows the maximum wind pressure obtained from Equation 10 ($g_f$ included), $\alpha$ equal to 0.15 and for varying values of $f_t$ (equal to 0.01, 0.1, 0.5 and 1 MPa from the bottom to the top). The dashed line is the maximum wind pressure obtained from Equation 6 ($g_f$ not included). The graph on the top right shows the same results but obtained for $\alpha$ equal to 0.05. The graph at the bottom shows that the curves obtained using Equation 6 and Equation 10 for $f_t$ =0.01 MPa give values that are within the range of Hamoush et al.'s [24] experimental data (shadowed area). This comparison shows that for masonry walls with negligible tensile strength,

both methods proposed in Equation 6 and 10 are suitable for predicting the ultimate wind pressure.

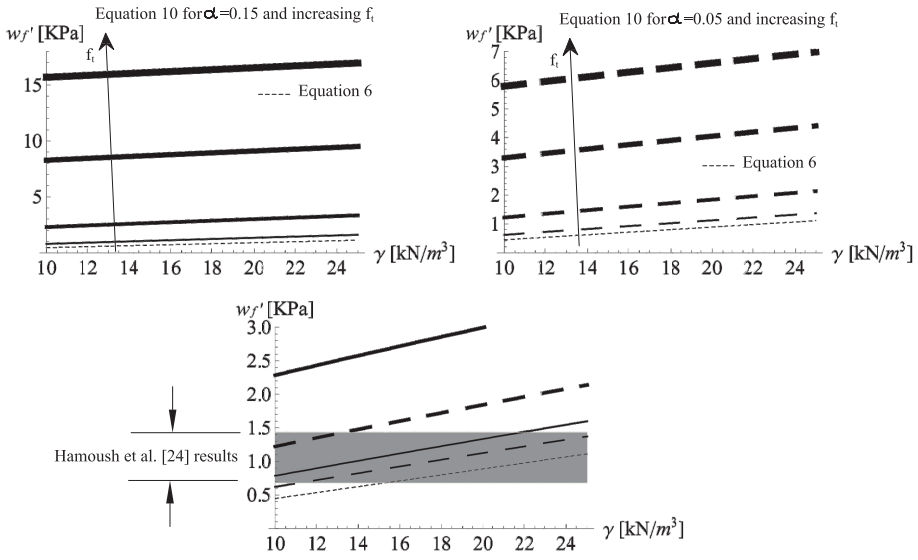


**Fig. 16** Comparison between the experimental data from Hamoush et al. [24] (shadowed area) and the analytical solution obtained from Equations 6 and 10 for increasing values of $f_t$ (0.01, 0.1, 0.5 and 1 MPa) and for $\alpha = 0.15$ (pn the left) and 0.05 (on the right).

A final comparison is presented against the procedure proposed by Morton [25]. Morton defines a failure mechanism similar to that shown in Figure 2 with the collapse dictated by the crushing of the extreme fibres under compression. Using this procedure, some analytical curves have been calculated by Hendry [26], for a masonry wall whose density is 16.77 $kN/m^3$, tensile strength $f_t$ = 0.35 MPa and different ratios of $P/td$. The results obtained using Equation 6 and using Equation 10 (for $f_t$=0.35 MPa and $\alpha$=0.15) are in very good agreement with the analytical curves obtained using Morton's procedure on Hendry's data, as shown in Figure 17.

## 6 Conclusions

The accuracy of elastic and ultimate strength analyses for the evaluation of the capacity of a rammed earth wall subject to lateral wind pressure have been assessed against the results of an experimental programme.

The elastic analysis has shown to be reasonably able to predict the maximum wind pressure that a wall can resist, and the position of the crack at failure. However, this method gives estimates that show errors up a 20% difference when compared with experimental results. The accuracy of the predic-

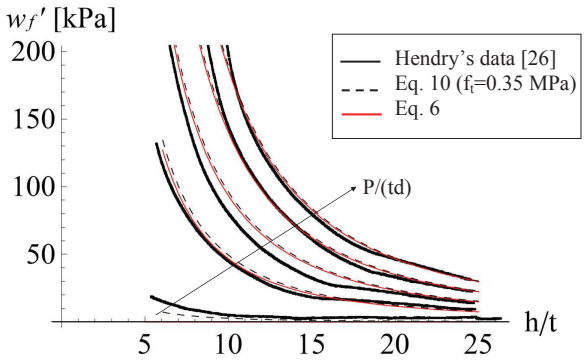


**Fig. 17** Comparison of the proposed methods in Eq. 6 and 10 with Hendry analytical results [26]: maximum wind pressure $w_f'$ vs. slenderness ratio h/t, for different values of precompression *P/(td)*=0,1,2,3 and 4 MPa.

tion seems to depend significantly on the determination of material mechanical properties such as the tensile strength $f_t$. The presented analytical methods correctly estimate the capacity of the wall to resist lateral wind pressure only when the assessment of the material properties is done rigorously, that is done under strictly controlled laboratory conditions. In reality the many variables in the experimental procedure of making rammed earth samples are difficult all to control. This aspect poses a limit to the accuracy of the analysis that might be overcome only with by increasing the comp[lexity of testing to unaffordable levels. The limitation of this analysis lies mainly in the assumption that the failure will happen at the location where the tensile stress is maximum, as shown for wall 3. If that location coincides with the weakest point in the wall, the assumption is reasonable and the method returns a precise valuation of the wall capacity. However, if the wall has a weaker point away from its central part (where usually stresses are higher), the method can overestimate the capacity of the wall, leading to dangerous results.

The ultimate strength analysis as presented in Equation 6 (i.e. without taking into account the contribution of the fracture energy required to open a crack) significantly underestimates the maximum wind pressure that the wall can sustain before failure. This method is recommended for the analysis of gravity or masonry walls, but is not recommended for the analysis of cement-stabilized rammed earth walls. This paper shows that the neglected effect of the fracture energy in the ultimate strength analysis might be the reason for the failure of this method in the prediction of the experimental behaviour. In this study, an ultimate strength analysis that includes the fracture energy of

the material reasonably predicts the maximum wind pressure that a wall can resist and the position of the crack at failure for *ad-hoc* assigned mechanical parameters. The approach is also shown to be applicable to masonry walls. Further investigation is needed to experimentally calculate these material parameters ($\alpha$, $\delta_{max}$ or simply $g_f$) of rammed earth. Another limitation of the proposed method is in the assumption that the crack will propagate through the entire thickness of the wall. For thicker walls, the mechanisms shown in Figure 13c might take place leading to a significantly different formulation. This case is currently a topic of research.

One last comment addresses the deterioration of the material properties through time due to aging and/or attack of external agents. The durability of the material goes beyond the purposes of this paper. However, it is appropriate to emphasize that the use of the presented design method does not take into consideration the lifespan of the structure and further work is needed in this area.

## 7 Acknowledgements

The authors would like to acknowledge the support of the Australian Research Council and the Department of Housing of the Government of Western Australia who provided financial assistance for this project (ARC Linkage Grant LP110100251). The first author would like to thank Varuni Wijewardane, Andrew Allsopp and Jim Waters for their help in the tiring and energy consuming ramming procedure of the experimental programme. She also would like to express her gratitude to Bill Smalley and Stephen Dobson for their help and collaboration in the discussion related to this paper.

## References

1. Elizabeth L, Adams C. Alternative Construction: Contemporary Natural Building Methods. John Wiley & Sons, New York; 2000.
2. Easton D. The Rammed Earth House. Chelsea Green Publishing Company, USA; 1996
3. Jaquin PA. Analysis of Historic Rammed Earth Construction. Ph.D thesis, University of Durham; 2008.
4. Jaquin PA, Augarde CE, Gallipoli D, Toll DG. The strength of unstabilised rammed earth materials, Geotechnique 2009; 59(5):487-490.
5. Middleton GF, Schneider LM. Bulletin 5: Earth-wall Construction, 4th edn, CSIRO, Sydney; 1987.
6. Walker P. Handbook 195: HB 195, Standards Australia International Ltd, Sydney; 2002.
7. Gale L. Building with earth bricks and rammed earth in Australia, Earth Buidling Association of Australia, Australia; 2005
8. Rima T. Design of Low-Rise Buildings for Extreme Wind Events, Journal of Architectural Engineering 2007; 13(1):54-62.
9. Griffith MC, Magenes G, Melis G, Picchi L. Evaluation of out-of-plane stability of unreinforced masonry walls subjected to seismic excitation. Journal of Earthquake Engineering 2003; 7(1):141-169.
10. Doherty K, Griffth MC, Lam N, Wilson J. Displacement-based seismic analysis for out-of-plane bending of unreinforced masonry walls. Earthquake Engng Struct. Dyn. 2002; 31:833-850.

11. Yttrup PJ. Strength of Earth Masonry (adobe) Walls Subjected to Lateral Wind Forces. In Seventh International Brick Masonry Conference, Australia 1985, p.981-991.
12. Ciancio D, Robinson S. Use of the strut-and-tie model in the analysis of reinforced cement-stabilised rammed earth. ASCE Journal of Materials in Civil Engineering 2011; 23(5):87-97.
13. Standards Australia, 1999, Methods of testing concrete: Method 9: Determination of the compressive strength of concrete specimens, AS 1012.09:1999, Standards Australia, Sydney.
14. Standards Australia, 2000a, Methods of testing concrete: Method 10: Determination of indirect tensile strength of concrete cylinders ("Brazil" or splitting test), AS 1012.10:2000, Standards Australia, Sydney.
15. ASTM International, 2008, Annual Book of ASTM Standards: Volume 04.02: Concrete and Aggregates, ASTM International, Pennsylvania.
16. Khaloo AR, Shooreh MRM, Askari SM. Size influence of specimens and maximum aggregate on dam concrete: Compressive strength, Journal of Materials in Civil Engineering 2009; 21(8):349355.
17. Ciancio D, Gibbings J. Experimental investigation on the compressive strength of cored and molded cement-stabilized rammed earth samples, Construction and Building Materials 2012; 28:294-304.
18. Hillerborg A. The theoretical basis of a method to determine the fracture energy Gf of concrete. Rilem Technical Committees, 0025-5432/85/04 291 06, Bordas-Gauthier-Villars.
19. Petersson PE. Fracture energy of concrete: energy of determination. Cement and Concrete Research 1980; 10:78-89.
20. Hillerborg A, Modeer M, Petersson PE. Analysis of crack formation and crack growth in concrete by means of fracture mechanics and finite elements, Cement and Concrete Research 1976; 6:773-782.
21. Guinea GV, El-Sayed K, Rocco CG, Elices M, Planas J. The effect of the bond between the matrix and the aggregates on the cracking mechanism and fracture parameters of concrete, Cement and Concrete Research 2001; 32:1961-1970.
22. Schlangen E, van Mier JGM. Experimental and Numerical Analysis of Micromechanisms of Fracture of Cement-Based Composites, Cement and Concrete Composites 1992; 14:105-118.
23. Petersson PE. Fracture Energy of concrete: practical performance and experimental results, Cement and Concrete Research 1980; 10:91-101.
24. Hamoush SA, McGinley MW, Mlakar P, Scott D, Murray K. Out-of-plane strengthening of masonry walls with reinforced composites, Journal of Composites for Construction 2001; 5(3): 139-145.
25. J. Morton. A theoretical and experimental investigation on the static and dynamic lateral resistance of brickwork panels with reference to damage gas explosion. PhD Thesis, University of Edinburgh; 1970.
26. Hendry AW. Structural Masonry, MacMillan Press LTD; 1998.